Supernovae producing unbound binaries and triples

C. S. Kochanek [1,2]★

[1]*Department of Astronomy, The Ohio State University, 140 West 18th Avenue, Columbus OH 43210, USA*
[2]*Center for Cosmology and AstroParticle Physics, The Ohio State University, 191 W. Woodruff Avenue, Columbus OH 43210, USA*

ABSTRACT

The fraction of stars that are in binaries or triples at the time of stellar death and the fraction of these systems that survive the supernova explosion are crucial constraints for evolution models and predictions for gravitational wave source populations. These fractions are also subject to direct observational determination. Here, we search 10 supernova remnants containing compact objects with proper motions for unbound binaries or triples using Gaia EDR3 and new statistical methods and tests for false positives. We confirm the one known example of an unbound binary, HD 37424 in G180.0−01.7, and find no other examples. Combining this with our previous searches for bound and unbound binaries, and assuming no bias in favour of finding interacting binaries, we find that 72.0 per cent (52.2–86.4 per cent, 90 per cent confidence) of supernova producing neutron stars are not binaries at the time of explosion, 13.9 per cent (5.4–27.2 per cent) produce bound binaries, and 12.5 per cent (2.8–31.3 per cent) produce unbound binaries. With a strong bias in favour of finding interacting binaries, the medians shift to 76.0 per cent were not binaries at death, 9.5 per cent leave bound binaries, and 13.2 per cent leave unbound binaries. Of explosions that do not leave binaries, <18.9 per cent can be fully unbound triples. These limits are conservatively for $M > 5\,\mathrm{M}_\odot$ companions, although the mass limits for some individual systems are significantly stronger. At birth, the progenitor of PSR J0538+2817 was probably a 13–19 $\mathrm{M}_\odot$ star, and at the time of explosion, it was probably a Roche limited, partially stripped star transferring mass to HD 37424 and then producing a Type IIL or IIb supernova.

Key words: stars: massive – supernovae: general – supernovae.

1 INTRODUCTION

Massive stars are not isolated. Almost all start in binaries (e.g. Kobulnicky & Fryer 2007; Sana et al. 2012; Moe & Di Stefano 2017; Villaseñor et al. 2021) and many are in triple or still higher order systems (Moe & Di Stefano 2017). The evolution of these systems is crucial to understanding the expected properties of supernovae (SN) and compact objects, and there is a long history of using binary population synthesis (BPS) models to try and follow the evolution of binary populations (e.g. Belczynski et al. 2008; Eldridge et al. 2017). These population studies have recently expanded to follow the evolution of triple or quadruple systems with their far richer dynamical properties (e.g. Toonen et al. 2020; Hamers et al. 2021). The end results for the evolution of massive star binaries and triples are particularly crucial (e.g. Belczynski, Kalogera & Bulik 2002; Kalogera et al. 2007, Dominik et al. 2013; Antonini, Toonen & Hamers 2017; Fragione & Kocsis 2019) to understanding the growing sample of compact object mergers found through gravitational-wave emission (e.g. Abbott et al. 2021).

While studies like Kobulnicky & Fryer (2007), Sana et al. (2012), Moe & Di Stefano (2017), and Villaseñor et al. (2021) are excellent surveys of the multiplicity of massive stars, the path to mergers or interacting compact objects is long and complex. In addition to standard problems in stellar evolution, there are the added problems

of mass transfer, common envelope evolution, neutron star (or black hole) birth kicks (see e.g. the review of BPS models by Han et al. 2020), and the nature of the mapping between core collapse and outcome (supernova or failed supernova, neutron star or black hole etc., see e.g. Kochanek 2014; Pejcha & Thompson 2015; Sukhbold et al. 2016). All of the physical effects are both uncertain and important for any prediction, including for the population of merging compact objects.

This process would be better constrained if we understood the multiplicity of systems containing compact objects and the fraction of initially multiple systems that survive the death of a member star. Compact object mergers, a small minority of the initial systems lying at the very end a complex evolutionary history, are likely a very poor way to understand this problem. Similarly, interacting neutron star and black hole binaries are a small biased fraction of binaries containing compact objects. Searches for non-interacting neutron star (other than pulsars) and black hole binaries are difficult and only just starting (e.g. Thompson et al. 2019, Jayasinghe et al. 2021) and searches for unbound compact objects only become fully practical as part of the microlensing component of the Roman Space Telescope (e.g. Lam et al. 2020).

There is, however, a second point in the evolution of these systems where it is possible to make progress. Studies of supernovae remnants (SNRs) can be used to determine the multiplicity of massive stars just before and after the death of a member. This was originally conceived of as a search for O/B stars associated with SNRs, potentially with peculiar kinematics (van den Bergh 1980; Guseinov, Ankay

★ E-mail: ckochanek@astronomy.ohio-state.edu

& Tagieva 2005). However, current models (e.g. Renzo et al. 2019) and data (e.g. Kochanek, Auchettl & Belczynski 2019) suggest that the kinematics of these stars are not very distinctive. None the less, given an estimate of the explosion site based on the centroid or expansion of the SNR, one can try to identify stars consistent with that location at the estimated time of explosion.

The easiest systems to examine are the very youngest SNRs: the Crab, Cas A, and SN 1987A. Because of their youth, the region that must be searched even for unbound companions is so small that it is trivial to rule out bound or unbound companions down to mass limits of $\sim M_\odot$ or less (Kochanek 2018, also see Kerzendorf et al. 2019 and Fraser & Boubert 2019). The lack of a companion in the Type IIb (Krause et al. 2008; Rest et al. 2011) SN Cas A is particularly interesting because models for producing Type IIb SNe typically rely on mass transfer (e.g. Benvenuto, Bersten & Nomoto 2013). The lack of a companion to SN 1987A is consistent with models of the progenitor as a merger remnant (e.g. Podsiadlowski 1992).

Older SNRs with identified compact remnants and limited extinction are easy to search for bound remnants simply using the properties of the optical counterpart to the neutron star. Kochanek et al. (2019) identified 23 Galactic SNRs where it was practical to carry out such a search, finding no non-interacting binaries and three previously identified interacting binaries. One of these systems, SS 433, is a Roche accreting system where the compact object is generally believed to be a black hole (see e.g. Hillwig & Gies 2008). The other two systems, HESS J0632+057 (Hinton et al. 2009) and 1FGL J1018.6−5856 (Corbet et al. 2011), are neutron star, wind accretion, and high-mass X-ray binaries (HMXBs). Kochanek et al. (2019) speculated that shock heating of the companion by the SN blast wave might drive it to have stronger winds for a period of time after the SN explosion, making it easier to produce such wind accretion systems. The lack of non-interacting binaries implied that fewer than 9.1 per cent (90 per cent confidence) of SN lead to such systems with a companion stellar mass $> 3\,M_\odot$.

Identifying unbound binaries or higher multiplicity systems in older SNRs is more challenging because the star and the stellar remnant are no longer co-located. van den Bergh (1980) appears to have carried out the first search, looking for an excess of O and B stars in 17 SNRs and finding none. Guseinov et al. (2005) examine 48 SNRs for O and B stars based on their magnitudes, colours, and proper motions, producing a list of candidates. Dinçel et al. (2015) identified the most promising candidate to date, HD 37424 in G180.0−0.17 by back-propagating the proper motions of the star and the pulsar to find that they intersect near the centre of the SNR. Boubert et al. (2017) examined 10 SNRs using the Tycho–*Gaia* astrometric solution (TGAS, Michalik, Lindegren & Hobbs 2015) proper motions to search for stars that passed close to the centres of the SNRs on reasonable time-scales. They identify four candidates, one of which is HD 37424. Lux et al. (2021) did the same for 12 SNRs using Gaia DR2 proper motions. Fraser & Boubert (2019) used Gaia DR2 proper motions for both the stars and the compact objects in the Crab, Cas A, and Vela SNRs, confirming the Kochanek (2018) result for the Crab and Cas A and finding only very low-luminosity candidates in Vela.

Because many SNRs are asymmetric and distorted, using an estimate of the centre of the SNR as an estimate of the explosion site is likely fraught for many SNRs unless a generous minimum distance is allowed to compensate for potential systematic problems. It is much safer to use the cases where a proper motion has been measured for the neutron star and we can simply search for intersections of the paths

Table 1. Remnants.

SNR	Centre	Radius ($'$)
G039.7−02.0	12:12:20+04:55:00	42.4
G069.0+02.7	19:54:50+33:00:30	40.0
G109.1−01.0	23:01:39+58:53:00	16.5
G130.7+03.1	02:05:34+64:49:50	4.2
G180.0−01.7	05:40:01+27:48:09	100.0
G205.5+00.5	06:39:00+06:30:00	110.0
G260.4−03.4	08:22:28−42:57:29	30.0
G263.9−03.3	08:35:21−45:10:35	249.0
G284.3−01.8	10:18:15−59:00:00	12.0
G296.5+10.0	12:09:40−52:25:00	38.0

of the star and the neutron star at some reasonable time in the past and distance from the centre. Here, we carry out this search for seven neutron stars and three interacting binaries associated with SNRs that have sufficiently good proper motion measurements to carry out a search. We describe the sample and our methods in Section 2. In particular, we describe methods to evaluate the probability of false positives both as a general assessment for each SNR and for particular stellar candidates. In Section 3, we present the results for unbound binaries. In Section 4, we extend the search to fully unbound triples. In Section 5, we consider the one candidate in more detail. We discuss the results in Section 6.

2 SEARCHING FOR UNBOUND SYSTEMS

The 10 SNRs we examine are summarized in Appendix A, and their properties are given in Tables 1 and 2. Only two of the single neutron stars have directly measured parallaxes. For the remaining five, we use rough distance estimates for the SNR expressed as parallaxes (see the discussion of the individual SNRs in the appendix). These were chosen so that a '1σ' change in the 'parallax' encompasses the estimated distances to the SNR. This is adopted as a convenient way to carry out the analysis, but these should not be regarded as true statistical uncertainties like those for the neutron stars with actual parallax measurements. For these cases, the 'parallax' entry in Table 2 is enclosed within parentheses. The three interacting binaries have *Gaia* proper motions and parallaxes.

We select nearby stars from Gaia EDR3 (Gaia Collaboration 2016; Gaia Collaboration 2021), requiring them to have proper motions, all three *Gaia* magnitudes (G, B_P and R_P) and $G < 18$ mag. We include no restrictions on the RUWE statistic for the quality of the parallax, and for the present effort, we can ignore the small systematic uncertainties in the parallax zero-point and the statistical differences between the inverse parallax and the distance. We are assuming that any unbound star has moved away from the compact object, which is a very safe assumption since even a 10 km s^{-1} velocity difference produces an angular separation of 2 arcsec at 10 kpc after 10^4 yr.

The bright $G \simeq 3$ magnitude limit of *Gaia* could be a problem for nearby SNRs because it may lead to the exclusion of the most luminous stars. We addressed this by also searching the *Hipparcos* (Perryman et al. 1997) and Bright Star (Hoffleit & Warren 1995) catalogues. For *Hipparcos*, we used the updated astrometric solution from van Leeuwen (2007). For the search regions used here, no bright stars were missing from the *Gaia* catalogue.

We used PARSEC (Bressan et al. 2012; Marigo et al. 2013; Pastorelli et al. 2020) isochrones to group the stars into mass ranges based on their locations in an extinction-corrected M_G versus $C = B_P - R_P$ colour magnitude diagram. This is the only part of the

Table 2. Compact object proper motions and parallaxes.

SNR	Position (J2000)	PM RA (mas yr^{-1})	PM Dec) (mas yr^{-1})	ϖ (mas)	Type
G039.7−02.0	19:11:49.565+04:58:57.82	− 3.027 ± 0.024	− 4.777 ± 0.024	0.118 ± 0.023	Binary, SS 433
G069.0+02.7	19:52:58.206+32:52:40.51	− 28.8 ± 0.9	− 14.7 ± 0.9	(0.75 ± 0.25)	Single
G109.1−01.0	23:01:08.295+58:52:44.45	− 6.4 ± 0.6	− 2.3 ± 0.6	(0.28 ± 0.05	Single
G130.7+03.1	02:05:37.922+64:49:41.33	− 1.40 ± 0.160	0.540 ± 0.575	(0.36 ± 0.14)	Single
G180.0−01.7	05:38:25.057+28:17:09.16	− 23.559 ± 0.085	52.766 ± 0.079	0.72 ± 0.12	Single
G205.5+00.5	06:32:59.257+05:48:01.16	− 0.026 ± 0.020	− 0.428 ± 0.016	0.540 ± 0.023	Binary, MWC 148
G260.4−03.4	08:21:57.274−43:00:17.33	− 74.2 ± 7.7	− 30.3 ± 6.2	(0.75 ± 0.25)	Single
G263.9−03.3	08:35:20.611−45:10:34.88	− 49.68 ± 0.06	29.90 ± 0.10	3.5 ± 0.2	Single
G284.3−01.8	10:18:55.587−58:56:45.98	− 6.454 ± 0.013	2.256 ± 0.010	0.227 ± 0.010	Binary, 2MASS J10185560−5856459
G296.5+10.0	12:10:00.913−52:26:28.30	− 12 ± 5	9 ± 8	(0.50 ± 0.25)	Single

Note. Parallaxes within parentheses are based on rough distance estimates not direct measurements.

Table 3. CMD selection limits.

Mass	Colour	Mag	Colour	Mag	Colour	Mag	Colour	Mag
>1 M$_\odot$	<1.5	5.5			1.5–2.0	$-1 - 3\,(B_P - R_P - 1)$	>2	−4
>2 M$_\odot$	<0.7	2.0	0.7–1.1	3.0	1.1–2.0	$-1 - 3\,(B_P - R_P - 1)$	>2	−4
>3 M$_\odot$	<0.7	1.0	0.7–1.1	2.0	1.1–2.0	$-1 - 3\,(B_P - R_P - 1)$	>2	−4
>4 M$_\odot$	<0.0	0.5	0.0–1.3	−1.9	1.3–2.0	$-1 - 3\,(B_P - R_P - 1)$	>2	−4
>5 M$_\odot$	<0.0	−0.4	0.0–1.3	−1.9	1.3–2.0	$-1 - 3\,(B_P - R_P - 1)$	>2	−4

Note. Mag gives the upper limit on M_G for each $B_P - R_P$ colour range.

calculation that uses distances, and simply using the inverse parallax here is sufficiently accurate because of the steepness of stellar mass-luminosity relations. We grouped them using limits of 1, 2, 3, 4, and 5 M$_\odot$, with the various colour-dependent absolute magnitude limits given in Table 3. As we noted in Kochanek et al. (2019), the lower mass stars will not yet be on the main sequence when the massive stars begin to explode as SN. These pre-main-sequence stars lie almost a full magnitude redwards in colour from the zero-age main sequence. The jump downwards in the magnitude limit near $C = B_P - R_P = 1$ is to ensure the inclusion of these pre-main-sequence stars. For higher mass stars, the 'dip' to fainter, redder pre-main-sequence stars is no longer necessary. For the >1 M$_\odot$ case, we also exclude stars with $-1 - 3\,(C - 1) < M_G < 3 + 5\,(C - 1)$ for $1.1 < C < 1.5$ to cut out the lower part of the red giant branch. The N_* column of Table 4 gives the number of stars above each $M_{\rm lim}$ that could have intersected the path of the neutron star in the last 10^5 yr at a velocity below 400 km s^{-1} (see below). Magnitude limits are becoming important when the number of stars stops rapidly increasing with $M_{\rm lim}$.

For extinction estimates, we used the three-dimensional com-bined19 mwdust models (Bovy et al. 2016), which combine the Drimmel, Cabrera-Lavers & López-Corredoira (2003), Marshall et al. (2006), and Green et al. (2019) models to provide extinction estimates for any sky position as a function of distance. We extracted the V-band extinction and used the PARSEC estimates of A_λ/A_V for the Gaia EDR3 bands and an $R_V = 3.1$ extinction law to convert the V-band extinction to those for the G, B_P, and R_P bands.

We first simply identify stars or pairs of stars whose parallaxes are consistent with the parallax of the neutron star. Given parallax estimates of $\varpi_i \pm \sigma_{\varpi,i}$ for $i = 1, 2$ (binary) or $i = 1, 2, 3$ (triple), we adopt the joint best-fitting parallax of

$$\varpi = \left[\sum_i \frac{\varpi_i}{\sigma_{\varpi,i}^2} \right] \left[\sum_i \frac{1}{\sigma_{\varpi,i}^2} \right]^{-1} \tag{1}$$

and the goodness of fit for this best-fitting parallax,

$$\chi_\varpi^2 = \sum_i \left(\frac{\varpi_i - \varpi}{\sigma_{\varpi,i}} \right)^2. \tag{2}$$

We initially keep all stars that as a potential binary companion satisfy $\chi_\varpi^2 < 9$. The exact cut is somewhat arbitrary but the goal is just to avoid wasting time on most of the stars that will never survive as candidates. For the neutron stars without direct parallaxes, we use the weak constraints based on estimates of the distance to the SNR discussed in the appendix.

Next, we restricted the sample to stars that could intersect the path of the neutron star in the time interval $-t_{\rm m} < t < 0$ at a stellar velocity less than $v_* < v_{\rm max}$. We again use a generous set of criteria because we are not yet using the actual stellar proper motions and their uncertainties, but this step does significantly reduce the numbers of stars that must be considered. We set $t_{\rm m} = 10^5$ yr and $v_{\rm max} = 400$ km s^{-1}. If the angular separation of the neutron star and the star is $\vec{\Delta\alpha} = \vec{\alpha}_{\rm ns} - \vec{\alpha}_*$ and the difference in proper motions is $\vec{\Delta\mu} = \vec{\mu}_{\rm ns} - \vec{\mu}_*$, then the physical projected separation is $\vec{\Delta x} = d\vec{\Delta\alpha}$ and the velocity difference is $\vec{v}_{\rm ns} = d\vec{\mu}_{\rm ns}$ where d is the distance. The stellar velocity v_* required to intercept the compact object at time t is

$$v_*^2(t) = v_{\rm ns}^2 + 2t^{-1}\vec{v}_{\rm ns} \cdot \vec{\Delta x} + \Delta x^2 t^{-2}, \tag{3}$$

which has a minimum of

$$v_{*\rm min}^2 = \frac{|\vec{\Delta x} \times \vec{v}_{\rm ns}|^2}{\Delta x^2} \tag{4}$$

at time

$$t_{*\rm min}^{-1} = -\frac{\vec{\Delta x} \cdot \vec{v}_{\rm ns}}{\Delta x^2}. \tag{5}$$

If the time of minimum velocity does not lie in the interval $-t_{\rm m} < t_{*\rm min} < 0$, then the minimum velocity for the star to intercept the compact object is just $v_*(-t_{\rm m})$, while if it does lie in the interval, the minimum velocity needed is $v_{*\rm min}$. The angular coordinate differences include

Table 4. Searching for disrupted binaries.

SNR	$M_{\lim}$ (M$_\odot$)	N_*	90% N_{obs}	N_{ran}	Prob.	95% N_{obs}	N_{ran}	Prob.	99% N_{obs}	N_{ran}	Prob.
G039.7−02.0	>5	953	0	0.0	–	0	0.0	–	0	0.0	–
	>4	957	0	0.0	–	0	0.0	–	0	0.0	–
	>3	2202	0	0.0	–	0	0.0	–	0	0.0	–
	>2	2527	0	0.0	–	0	0.0	–	0	0.0	–
	>1	2641	0	0.0	–	0	0.0	–	0	0.0	–
G069.0+02.7	>5	1382	0	0.1	–	0	0.2	–	2	0.7	16%
	>4	1421	0	0.1	–	0	0.3	–	2	0.9	23%
	>3	5178	2	1.9	55%	3	3.2	61%	20	14.9	12%
	>2	9158	9	7.8	38%	19	15.1	19%	56	46.6	10%
	>1	23748	66	83.7	98%	111	128.6	95%	213	227.5	84%
G109.1−01.0	>5	26	0	0.1	–	0	0.1	–	0	0.2	–
	>4	33	0	0.2	–	0	0.2	–	0	0.4	–
	>3	243	1	1.2	71%	2	1.8	52%	3	2.8	53%
	>2	519	1	1.2	71%	2	1.8	52%	3	2.8	53%
	>1	1741	1	1.2	71%	2	1.8	52%	3	2.8	53%
G130.7+03.1	>5	5	0	0.0	–	0	0.0	–	0	0.0	–
	>4	5	0	0.0	–	0	0.0	–	0	0.0	–
	>3	69	0	0.0	–	0	0.0	–	0	0.0	–
	>2	155	0	0.0	–	0	0.0	–	0	0.0	–
	>1	361	0	0.0	–	0	0.0	–	0	0.0	–
G180.0−01.7	>5	0	1	0.0	0%	1	0.0	0%	1	0.0	3%
	>4	0	1	0.0	2%	1	0.0	3%	1	0.1	7%
	>3	0	1	0.2	18%	1	0.3	24%	1	0.5	39%
	>2	29	2	0.8	18%	2	1.1	29%	2	1.9	55%
	>1	8973	8	9.7	75%	9	13.6	92%	18	20.9	77%
G205.5+00.5	>5	37	0	0.0	–	0	0.0	–	0	0.0	–
	>4	54	0	0.0	–	0	0.0	–	0	0.0	–
	>3	272	0	0.0	–	0	0.0	–	0	0.0	–
	>2	1067	0	0.0	–	0	0.0	–	0	0.0	–
	>1	11860	0	0.0	–	0	0.0	–	0	0.0	–
G260.4−03.4	>5	147	0	0.2	–	0	0.3	–	0	0.7	–
	>4	168	0	0.6	–	0	0.7	–	0	1.2	–
	>3	658	0	1.9	–	1	2.8	94%	8	5.6	20%
	>2	1079	4	5.7	82%	6	7.8	79%	14	12.2	34%
	>1	2679	28	31.8	77%	35	39.4	78%	54	54.4	54%
G263.9−03.3	>5	5	0	0.0	–	0	0.0	–	0	0.0	–
	>4	16	0	0.0	–	0	0.0	–	0	0.0	–
	>3	45	0	0.0	–	0	0.0	–	0	0.0	–
	>2	97	0	0.0	–	0	0.0	–	0	0.0	–
	>1	963	0	0.2	–	0	0.3	–	0	0.4	–
G284.3−01.8	>5	322	0	0.0	–	0	0.0	–	0	0.0	–
	>4	539	0	0.0	–	0	0.0	–	0	0.0	–
	>3	1394	0	0.0	–	0	0.0	–	0	0.0	–
	>2	2016	0	0.0	–	0	0.0	–	0	0.0	–
	>1	2439	0	0.0	–	0	0.0	–	0	0.0	–
G296.5+10.0	>5	63	0	0.0	–	0	0.0	–	0	0.0	–
	>4	63	0	0.0	–	0	0.0	–	0	0.0	–
	>3	606	0	0.2	–	0	0.3	–	0	0.3	–
	>2	1305	2	0.8	21%	2	1.1	30%	2	1.3	37%
	>1	8372	15	13.9	42%	18	15.8	33%	22	17.5	17%

the necessary $\cos\delta$ term for the separation in RA, and the positions of the stars passing the criteria are close enough to the neutron star that we need not do a full spherical trigonometry calculation.

We do not want to restrict our search to stars that can exactly intersect the neutron star at a particular time. If we allow binary separations of $a_{\max}$, then a star need only pass within the angular distance

$$\sigma_a = 10\overset{''}{.}0 \left(\frac{a_{\max}}{10^4\,\mathrm{AU}} \right) \left(\frac{\varpi}{\mathrm{mas}} \right) \tag{6}$$

to potentially have been a binary companion of the neutron star. So, we need a method that accounts for both the uncertainties in

the proper motions and a finite angular separation at the time of explosion. We can account for both by introducing the true proper motions of the objects as an intermediate variable. Consider the motion in RA. Let the position separation be $\Delta\alpha_{12} = \alpha_1 - \alpha_2$ (the $\cos\delta$ is again implicit, and 1 and 2 refer to the neutron star and the star), the measured proper motions in RA be $\mu_{\alpha,i}$, and the true proper motions in RA be $\mu_{\alpha,i}^T$. The true proper motion is constrained by the measured proper motions, and the separation as a function of time then depends on $\Delta\alpha_{12} - t(\mu_{\alpha,1}^T - \mu_{\alpha,2}^T)$. This leads to the fit statistic

$$\chi^2_{\alpha,12} = \frac{\left(\mu_{\alpha,1} - \mu_{\alpha,1}^T\right)^2}{\sigma_{\alpha,1}^2} + \frac{\left(\mu_{\alpha,2} - \mu_{\alpha,2}^T\right)^2}{\sigma_{\alpha,2}^2} + \frac{\left(\Delta\alpha_{12} - t(\mu_{\alpha,1}^T - \mu_{\alpha,2}^T)\right)^2}{\sigma_a^2}, \tag{7}$$

where the first two terms constrain the true proper motions using the measured proper motions and the last term constrains the closest approach, given the true proper motions. If we optimize the statistic with respect to the unknown true proper motions,

$$\chi^2_{\alpha,12} = \frac{(\Delta\alpha_{12}/t - \Delta\mu_{\alpha,12})^2}{\sigma_{\alpha,12}^2}, \tag{8}$$

where $\Delta\mu_{\alpha,12} = \mu_{\alpha,1} - \mu_{\alpha,2}$, and

$$\sigma_{\alpha,12}^2 = \sigma_{\alpha,1}^2 + \sigma_{\alpha,2}^2 + \sigma_a^2/t^2. \tag{9}$$

If we now define $\Delta_{\alpha,12} = \Delta\alpha_{12}/t - \Delta\mu_{\alpha,12}$, then the overall statistic is

$$\chi^2_\mu = \frac{\Delta_{\alpha,12}^2}{\sigma_{\alpha,12}^2} + \frac{\Delta_{\delta,12}^2}{\sigma_{\delta,12}^2}, \tag{10}$$

after including the analogous term in Declination. In essence, a $\chi^2_\mu \simeq 3$ means that the star can pass within distance a_{max} of the neutron star using proper motions that are each within 1σ of the measured values. While the optimization of χ^2_μ is formally non-linear in t^{-1} due to equation (9), the problem is easily solved iteratively: fix the time in equation (9) to determine a new optimal time, use this time to update equation (9), and repeat. The ratio $t\sigma_\mu/\sigma_a$ of the two terms in equation (9) indicates whether the position uncertainty due to the proper motions at closest approach ($t_m\sigma_\mu$) is larger ($t_m\sigma_\mu/\sigma_a > 1$) or smaller ($t_m\sigma_\mu/\sigma_a < 1$) than the desired maximum separation σ_a. While we do not include the position uncertainties because they are unimportant, they can be included as an error term like σ_a.

With the uncertainties fixed, the closest approach time is

$$t_m = -\frac{\Delta\alpha_{12}^2\sigma_{\delta,12}^2 + \Delta\delta_{12}^2\sigma_{\alpha,12}^2}{\Delta\alpha_{12}\Delta\mu_{\alpha,12}\sigma_{\delta,12}^2 + \Delta\delta_{12}\Delta\mu_{\delta,12}\sigma_{\alpha,12}^2} \tag{11}$$

with a goodness of fit

$$\chi^2_{12} = \frac{(\Delta\delta_{12}\Delta\mu_{\alpha,12} - \Delta\alpha_{12}\Delta\mu_{\delta,12})^2}{\Delta\alpha_{12}^2\sigma_{\delta,12}^2 + \Delta\delta_{12}^2\sigma_{\alpha,12}^2}. \tag{12}$$

For equal uncertainties, the goodness of fit is basically just the amplitude of the proper motions perpendicular to the separation vector relative to the proper motion uncertainties, squared.

We use the same procedure to search for triples. The overall fit statistic replacing the first term of equation (10) is

$$\chi^2_\alpha = \frac{\sigma_{\alpha,3}^2\Delta_{\alpha,12}^2 + \sigma_{\alpha,2}^2\Delta_{\alpha,13}^2 + \sigma_{\alpha,1}^2\Delta_{\alpha,23}^2}{\sigma_{\alpha,1}^2\sigma_{\alpha,2}^2 + \sigma_{\alpha,1}^2\sigma_{\alpha,3}^2 + \sigma_{\alpha,2}^2\sigma_{\alpha,3}^2} \tag{13}$$

with an equivalent term for the Declination where 1, 2, and 3 are the neutron star, the first star, and the second star, respectively. The definitions of the errors $\sigma_{\alpha,i}$ depend on how we want to restrict the

separations. If we want to restrict only the minimum distance of the stars from the neutron star, then the uncertainties are $\sigma_{\alpha,1}$ for the neutron star and $\sigma_{\alpha,i}^2 \rightarrow \sigma_{\alpha,i}^2 + \sigma_a^2/t^2$ for each of the two stars. Equation (13) then becomes identical to equation (10) in the limit of making the proper motion uncertainties of one of the stars infinite. If you also add a term constraining the separation of the two stars by σ_a, then the uncertainties are $\sigma_{\alpha,i}^2 \rightarrow \sigma_{\alpha,i}^2 + \sigma_a^2/3t^2$ for all three objects. Here, we use this latter form. The solution is again found by iteratively holding the uncertainties fixed, solving for t_m, and updating the uncertainties.

We consider the problem of false positives in two ways. First, we generally characterize each SNR by scrambling the stellar positions relative to their magnitudes, proper motions, and parallaxes. We keep the latter three quantities tied because the uncertainties in the proper motions and parallaxes are in large part determined by the magnitude. While this is also true of the uncertainties in the positions, the position uncertainties are unimportant compared to the proper motion uncertainties and can be regarded as fixed. For each trial, we assigned a random number to each star and assigned positions in the order of these random numbers. So, if star #1 appeared as the 50th entry in this list, it was assigned the position of star #50. We rejected the occasional cases where a star would be assigned its true position, but we did not try to eliminate the occasional cases where multiple trials would consider the same random pairing. With $N_* \simeq 4000$ stars and $N_t = 100$ trials, there are $N_*N_t \simeq 400\,000$ random pairings of the neutron star with single stars of which we expect only ~100 duplicates. We do $N_t = 100$ random trials for each SNR and count the number of candidates that have a position of closest approach inside 20 per cent of the SNR radius and $\chi^2_\varpi + \chi^2_\mu$ smaller than several threshold values.

We can also evaluate the likelihood that a particular candidate is a false positive. This can be very different than the general probability of a false positive if a candidate has an unusual proper motion. For example, if a candidate has a relatively high proper motion compared to the rest of the stars, then it is unlikely that a different randomly selected proper motion will work. To try to quantify this, we take all stars with $\chi^2_\varpi < 9$ and within 1 mag of each candidate unbound binary star and put it at the position of the candidate. We restrict the magnitude range so that the stars have similar kinematics and proper motion uncertainties. We then determine the fraction of these trials, which would produce a $\chi^2_\varpi + \chi^2_\mu$ goodness of fit less than the larger of the fit statistic of the candidate or 2.706 (90 per cent confidence). The second criterion is included to cover a scenario in which a candidate has a very small fit statistic (say $\chi^2_\varpi + \chi^2_\mu = 0$ in the limit of perfection) but many random trials are also leading to very good fit statistics (<2.706) – such a case should still be regarded as having a high false-positive probability.

We evaluate these two false-positive statistics at the level of unbound binaries. Since all unbound triple candidates will consist of two unbound binary candidates, SNRs that have large false-positive rates for unbound binaries will also be the ones with high false-positive rates for triples. Similarly, all unbound triple candidates will comprise two unbound binary candidates, so if one or both of the binary candidates have a high false-positive probability, then the unbound triple candidate has a high false-positive probability.

3 BINARIES

Table 4 summarizes the overall statistics of searching for unbound stars in each of the SNRs. For probability limits of 90 per cent ($\chi^2_\varpi + \chi^2_\mu < 2.706$), 95 per cent (3.841), and 99 per cent (6.635), the table gives the number of stars considered, N_*, the number of actual

Table 5. Disrupted binary candidates.

SNR	Gaia EDR3 ID	M_{lim} ($M_\odot$)	False (%)	χ^2_ϖ	χ^2_μ	t_{min} (10^3 yr)	R/R_{SNR}	ϖ (mas)	Comment
G069.0+02.7	2034331673776151552	5	49	3.858	0.062	− 57.7	0.19	0.259 ± 0.010	
	2034320300712461184	5	54	4.151	0.461	− 36.7	0.15	0.242 ± 0.017	
G109.1−01.0	2013340789887658240	3	4	3.073	0.368	− 53.0	0.15	0.365 ± 0.012	
	2013340381858998016	3	64	3.479	1.284	− 53.6	0.15	0.210 ± 0.033	
	2013340175700592384	3	41	1.220	1.178	− 56.6	0.17	0.330 ± 0.022	
G180.0−01.7	3441732292729818752	5	0	0.282	0.261	− 29.3	0.10	0.658 ± 0.028	HD37424
	3441706518633166080	2	14	0.433	0.048	− 48.7	0.14	0.798 ± 0.018	
G260.4−03.4	5526330988095223552	3	100	3.890	0.501	− 7.3	0.12	0.268 ± 0.052	
	5526330472698907904	3	100	5.723	0.026	− 5.5	0.04	0.167 ± 0.055	
	5526330403979671552	3	100	6.161	0.343	− 7.0	0.11	0.156 ± 0.072	
	5526325387457616128	3	100	3.051	0.310	− 4.0	0.03	0.321 ± 0.046	
	5526325284378390272	3	99	5.250	0.006	− 2.0	0.12	0.181 ± 0.029	
	5526325284378390144	3	99	3.631	0.309	− 2.4	0.10	0.280 ± 0.042	
	5526319099625741184	3	78	4.923	0.007	− 9.0	0.19	0.208 ± 0.054	
	5526319095324073856	3	94	5.814	0.011	− 8.7	0.18	0.189 ± 0.091	
G296.5+10.0	6125329220509401984	2	41	0.011	1.480	− 10.2	0.16	0.474 ± 0.030	
	6125328945636431104	2	76	2.250	0.128	− 14.8	0.19	0.152 ± 0.093	

candidates, N_{obs}, the average number of random candidates found per trial, N_{ran}, and the Poisson likelihood of finding N_{obs} or more candidates, given an expectation value of N_{ran}, all as function of the minimum mass selection limit M_{lim}. The probability is meaningless for a bin with $N_{obs} = 0$, so no probability is given for these bins. These are all for $R/R_{SNR} < 0.2$, $a_{max} = 10^4$ AU and $t_{min} > -10^5$ yr. Note that there is little benefit from limiting the search to more compact binaries (smaller a_{max}) because this scale does not matter once it is smaller than the position uncertainties created by back propagating the proper motions for tens of thousands of years.

Even without the detailed numbers, the visual appearance of Table 4 shows that these SNRs span a range of statistical properties. Some, like G263.9−03.3, show large numbers of zeroes indicating that there is almost no chance of finding a false positive independent of the mass limit or the statistical threshold. This illustrates the advantage of having an accurate neutron star parallax rather than a rough distance estimate for the SNR. Others, like G069.0+02.7, show rapidly rising numbers of candidates as the mass limit is lowered or the statistical threshold is weakened but have matching numbers of predicted false positives. This is a consequence of the lack of a direct parallax for the neutron star and a higher projected stellar density. The expected number of false positives rises as the mass limit is lowered because both the number of stars and the uncertainties in the *Gaia* parallaxes and proper motions increase, and it increases as the probability threshold is weakened. The number of observed candidates tracks the expected number from the random realizations extremely well, so the Poisson probabilities of finding at least as many candidates as observed are almost always significant. In fact, the only SNR with a candidate that is very unlikely to be a false positive is G180.0−01.7, and this is the Dinçel et al. (2015) candidate HD 37424.

Since we are primarily interested in the more massive companions, we examined the candidates in the highest mass limit with candidates for each SNR, with the exception of G180.0−01.7, where we use the mass limit producing a second candidate besides HD 37424. The properties of these candidates are given in Table 5. SNRs with no candidates are not included. In Table 5, we include the probability of obtaining a $\chi^2_\varpi + \chi^2_\mu$ value less than the larger of 2.706 and the

actual value when assigning the same position the parallaxes and proper motions of some other star within ±1 G mag of the candidate. Essentially, all the candidates except HD 37424 have positions that produce equally good or better fit statistics for significant fractions of randomly selected proper motions.

In the end, we reject all the candidates in Table 5 except HD 37424. The two candidates in G069.0+02.7 have high false-positive probabilities, their distances imply that they are well behind the SNR, and the intercept times are somewhat young. These candidates pass the fit statistic requirements because of how we converted the distance estimate to the SNR (1–2 kpc, see appendix) into a χ^2_ϖ with $\varpi = 0.75 \pm 0.25$ mas to characterize the distance match. With this choice, $\chi^2_\varpi = 1$ at the two limiting distance estimates of 1 and 2 kpc. The two candidates have $\varpi \simeq 0.25$ mas, which leads to $\chi^2_\varpi \simeq 4$ in Table 5 and the formal inclusion of the two stars as candidates. However, their parallaxes correspond to a distance of 4 kpc that is well behind the SNR unless the distance estimates for G069.0+02.7 are completely wrong. Using χ^2_ϖ defined in this manner for the SNRs without parallax distances to the remnants is a simple approach, but it should not be interpreted literally in terms of Gaussian statistics when it comes to rejecting candidates.

This is a consideration for the other SNRs without direct parallaxes. For G109.1−01.0, one candidate does have a low false-positive probability (4 per cent), but the parallaxes are all somewhat high or low and the intercept times are too old. The lower mass cut star we kept in G180.0−01.7 has a 14 per cent false-positive probability and an intercept time that is too old. G260.4−03.4 has a large number of lower mass candidates, all of which have very high false-positive rates. Many of the parallaxes imply distances that are likely behind the SNR, although several have intercept times consistent with estimates for the age of the SNR. G296.5+10.0 has two candidates with high false-positive probabilities but ages and parallaxes more or less consistent with estimates for the SNR. G130.7+03.1 and G263.9−03.3 have no candidates even for the $>1 M_\odot$ mass cut.

Our various false-positive tests make it clear that you will find candidates associated with any SNR if you search enough stars. The candidates in Table 5 come from going to lower and lower mass limits

Table 6. Disrupted triple candidates.

SNR	Gaia EDR3 ID	$M_{\rm lim}$ ($M_\odot$)	False (%)	χ^2_ϖ	χ^2_μ	$t_{\rm min}$ (10^3 yr)	$R/R_{\rm SNR}$	ϖ (mas)	Comment
G069.0+02.7	2034319682237156096, 2034319510438472320	3,3	66, 68	5.689	1.047	−42.6	0.10	0.197 ± 0.018	
	2034331570696943232, 2034330952221647232	3,2	65, 30	4.817	3.804	−52.6	0.13	0.271 ± 0.021	
	2034342943771429504, 2034329848377469824	3,1	72, 1	3.994	1.831	−53.9	0.15	0.344 ± 0.022	
	2034342943771428992, 2034331227099572480	3,1	56, 65	3.303	3.225	−49.4	0.11	0.447 ± 0.012	
	2034342943771428992, 2034319299937887872	3,1	56, 42	1.804	7.166	−47.4	0.10	0.436 ± 0.014	
G180.0−01.7	3441732292729818752, 3442478238354719872	5,1	0, 35	0.283	1.769	−29.3	0.10	0.658 ± 0.026	HD37424
G260.4−03.4	5526325353097874176, 5526325250018655616	2,2	99, 98	1.189	6.940	−3.2	0.07	0.667 ± 0.008	
G296.5+10.0	6125329220509401984, 6125328911271728768	2,1	41, 92	2.128	4.753	−10.0	0.16	0.496 ± 0.026	

until there are candidates. They almost all have high false-positive probabilities, so they are almost all likely to be false positives other than HD 37424. However, with the available data and uncertainties, we cannot definitively prove this for particular stars. What we can conclude is that in this sample of 10 SNRs, there is only one unbound companion with a mass $>5\,M_\odot$, as we do think that it is reasonable to exclude the two candidates associated with G069.0+02.7.

The unbound star search for the three SNRs with binaries is really a search for triple systems in which one star remains bound to the compact object and the other star becomes unbound. We find no such candidates for G039.7−02.0 (SS 433), G205.5+00.5 (HESS J0632+05 and MWC 148), or G284.3−01.8 (1FGL J1018.6−5856 and 2MASS J10185560−5856459). For SS 433, we carried out the search both for the Gaia EDR3 parallax and for the distances estimated from kinematic models of SS 433 by Blundell & Bowler (2004) and Marshall et al. (2013). Table 4 gives the results for the *Gaia* parallax distance. The limits for SS 433 should only be regarded as holding for $>5\,M_\odot$ due to its larger distance and extinction compared to the other SNRs we consider. We can clearly reject the candidate HD 261393 found for G205.5+00.5 by Boubert et al. (2017). Its Gaia EDR3 parallax of $\varpi = 0.923 \pm 0.025$ mas is inconsistent with that of MWC 148 ($\varpi = 0.540 \pm 0.023$ mas) at $\sim 130\sigma$. The remaining Lux et al. (2021) candidates in this SNR also have parallaxes incompatible with MWC 148.

4 DISRUPTED TRIPLES

For the SNRs with single neutron stars, we can carry out the search for fully disrupted triples. We now keep candidates with $\chi^2_\varpi + \chi^2_\mu < 9.210$ and allow pairings including all stars meeting the $>1\,M_\odot$ mass cut. Because the two stars must have similar parallaxes and proper motions that intersect within 10^5 yr and $R/R_{\rm SNR} < 0.2$, the problem of false positives is greatly reduced over the search for unbound binaries. None the less, it is still simply a question of how low a mass limit can be used before you have significant probabilities of false positives, not whether you will have false positives once you include enough stars.

The candidates are listed in Table 6. There are now only four SNRs with candidates despite the relaxed mass limits. Except for HD 37424, they all have high false-positive probabilities, and G069.0+02.7 again has the most. Basically, since G069.0+02.7 has the largest number of stars that are unbound binary candidates, it is also much more likely that two of these candidates can have similar parallaxes and intercept times. Most of the candidates have rather high values for their $\chi^2_\varpi + \chi^2_\mu$ fit statistic.

Curiously, the best candidate again involves HD 37424, where there is a much lower mass star ($M_{\rm lim} > 1\,M_\odot$) with a consistent

distance ($\chi^2_\varpi = 0.3$) and a good ($\chi^2_\mu = 1.8$), simultaneous intercept with the NS 29 000 yr ago close to the centre of the remnant ($R/R_{\rm SNR} = 0.1$). It does, however, have a significant false-positive probability. Its kinematics would allow it to be in a wide binary with the neutron star progenitor and HD 37424. In the local standard of rest (see below in Section 5), its proper motion corresponds to a velocity of ~ 22 km s^{-1} as compared to ~ 95 km s^{-1} for HD 37424. If we view these as circular velocities and assume that the neutron star progenitor and HD 37424 had similar masses, this would make the semimajor axis of the outer binary ~ 40 times that of the inner binary. Of course, the actual ratio would depend on the orbital phases at the time of explosion and the degree to which the system lay in the plane of the sky. There will, however, be a tendency for slower moving stars coincidentally close to the explosion site to produce false positives because the actual direction of their motions becomes relatively unimportant.

Like the examples of unbound binary candidates, we cannot prove that the unbound triple candidates in Table 6 are all false positives, although it seems likely. What we can say is that these seven SNRs contain no examples of disrupted massive star triple systems. Conservatively, none of these neutron stars was in a triple containing two $>5\,M_\odot$ stars in addition to the SN progenitor.

5 HD 37424 AND PSR J0538+2817

Fig. 1 shows a *Gaia* colour-magnitude diagram (CMD) of all stars with parallaxes of $0.581 < \varpi < 0.758$ mas, which is nominally ± 200 pc around the joint parallax ($\varpi = 0.658 \pm 0.028$ mas, or 1.52 kpc) of HD 37424 and the neutron star, angles $<3.77°$ from the centre of the SNR, which is 100 pc at the nominal distance, and with $G < 10$ mag (1 mag fainter than HD 37424). This yielded a sample of 50 stars. If we compare these stars to the PARSEC isochrones with $\log t = 6.6, 7.0, 7.5, 8.0$, and 8.5, we see that they are all consistent with $\log t \gtrsim 7.5$, and the initial mass of the most massive stars remaining on this isochrone is $9.1\,M_\odot$. There are certainly no stars close to the $\log t = 7.0$ isochrone where the initial mass of the most massive remaining star is $19.3\,M_\odot$.

At the absolute magnitude of HD 37424, the $\log t \lesssim 7$ isochrones are nearly vertical, so any estimate of its age is largely determined by its colour. Dinçel et al. (2015) spectroscopically classified HD 37424 as a B0.5V star and estimated a mass and luminosity of $M_* \simeq 13\,M_\odot$ and $L_* \simeq 14000 L_\odot$ based on the calibrations of spectral types by Hohle, Neuhäuser & Schutz (2010).

We can construct a spectral energy distribution (SED) for HD 37424 spanning from 1570 Å to 4.6 µm using UV fluxes from Thompson et al. (1978), optical fluxes from NOMAD (Zacharias et al. 2005), near-IR fluxes from 2MASS (Skrutskie et al. 2006),
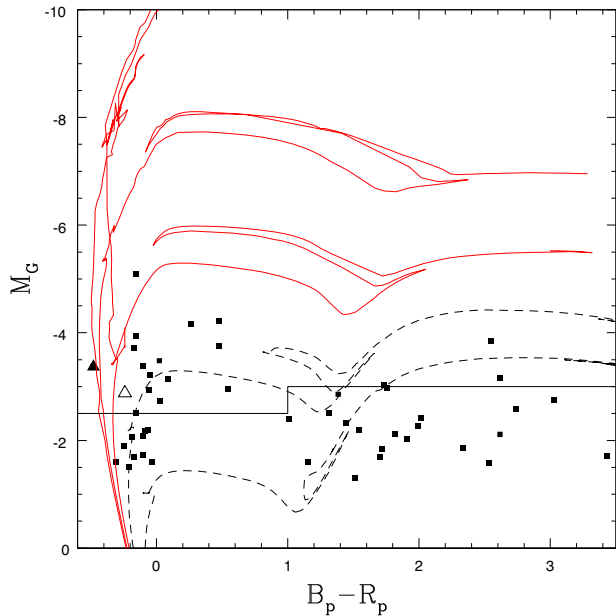
Figure 1. Extinction-corrected CMD of stars with $G < 10$ mag within ± 200 pc along the line of sight and 100 pc in the plane of the sky of G180.0−01.7. The large filled (open) triangle is HD 37424 based on the mwdust (SED fit) extinction estimate. The red solid PARSEC isochrones are for $\log t = 6.6$, 7.0, and 7.5, while the black dashed isochrones are for $\log t = 8.0$ and 8.5. The maximum initial masses for stars remaining on the $\log t = 7.0$, 7.5, 8.0, and 8.5 isochrones are 19.3, 9.1, 5.3, and $3.4 \, \mathrm{M_\odot}$, respectively. The SED models for the 18 stars above the horizontal lines are presented in Table 7.

and mid-IR fluxes from AllWise (Cutri et al. 2012). We used a temperature prior of $T_* = 26\,000 \pm 3000$ K based on the spectral type, and an extinction prior of $E(B - V) = 0.5 \pm 0.1$ based on the mwdust extinction estimate. The photometric errors were set to be the larger of the reported uncertainties and 10 per cent with the exception of the 2740-Å UV flux. The error for this band was set to 30 per cent because it markedly disagrees with any smooth SED. The minimum photometric uncertainty is to compensate for systematic uncertainties. We fit the SED using Markov Chain Monte Carlo methods and Solar metallicity Castelli & Kurucz (2003) atmosphere models to find that $T_* = 27\,000 \pm 2600$ K, $L_* = 16\,600 \pm 4500 L_\odot$, $R_* = 5.9 \pm 0.3 R_\odot$, and $E(B - V) = 0.34 \pm 0.04$. The goodness of fit is reasonable, with $\chi^2 = 9.7$ for 11 degrees of freedom (12 photometric measurements, two priors, and three variables). The SED slightly constrains the temperature over the prior from the spectral type (B9). The SED requires less extinction than the mwdust estimate, which shifts the star redwards to colours more typical of the other nearby massive stars (see Fig. 1).

If we search for models with these luminosities and temperatures in the Solar metallicity PARSEC isochrones, we can estimate the mass and age of the system. We selected models using a χ^2 statistic to measure the distance of the model from the estimated stellar parameters and simply tracked the maximum and minimum values within a given χ^2 limit. In matching to the isochrones, we used the larger of the estimated uncertainties and 5 per cent or 10 per cent for the temperature and luminosity, respectively. For $\chi^2 < 1$, the current mass and age ranges were $11.1 \, \mathrm{M_\odot} < M_* < 13.9 \, \mathrm{M_\odot}$ and $\log t < 7.18$, while for $\chi^2 < 4$, the ranges were $10.0 \, \mathrm{M_\odot} < M_* < 15.3 \, \mathrm{M_\odot}$ and $\log t < 7.38$. There was no useful lower limit on the age. The upper age limits are certainly consistent with the star being

the companion of a supernova, as the maximum initial masses for the $\log t = 7.18$ and 7.38 isochrones are $14.0 \, \mathrm{M_\odot}$ and $10.6 \, \mathrm{M_\odot}$, respectively. These parameters are summarized in Table 7.

We also modelled the SEDs of the 18 stars with mwdust extinction-corrected absolute magnitudes of $M_G < -2.5$ ($M_G < -3.0$) and $B_P - R_P < 1$ (> 1). The limit on the blue main sequence is faint enough to include all stars, which might eventually undergo core collapse, and the modest shift upwards in luminosity for redder colours was designed so that a few lower mass red giants were included to provide a check that they were lower mass without having to model many of them. This selection limit is shown in Fig. 1. For the red giants, we generally used APASS (Henden et al. 2016) instead of NOMAD for the optical magnitudes and the MARCS (Gustafsson et al. 2008) atmosphere models. We had to broaden the photometric uncertainties of some bands to 20–30 per cent to reach a reasonable χ^2/N_{dof}. All the hotter stars had UV fluxes from Thompson et al. (1978), which provided enough temperature information to make it clear that the hottest stars were B and not O stars, consistent with the reported spectral types. This also allowed very robust individual extinction estimates. Table 7 reports the resulting temperatures and luminosities along with the $\chi^2 < 4$ range of PARSEC isochrone initial masses and ages to which they could correspond. The luminosities, temperatures, masses, and ages of these stars, along with their spectral types and any interesting properties in the SIMBAD (Wenger et al. 2000) data base, are also given in Table 7 and sorted by luminosity.

Most of the stars shift very little in the CMD with the directly estimated extinctions. The exception is TIC 3219130 where the mwdust extinction estimate of $E(B - V) = 0.98$ is much too high – the SED implies $E(B - V) = 0.31$, which makes the star a rather low-mass red giant. The other two red giants (V339 Aur and TIC 76026324) are also relatively low mass, consistent with their locations on the CMD. The temperature estimates from the SEDs are generally consistent with the spectroscopic classifications with the exception of V1164 Tau.

SIMBAD flags three stars as variables, V1164 Tau, ET Tau, and V399 Aur. The classification of V1164 Tau as an ellipsoidal variable (ell) is from an automated classifier with no detailed analysis. As a luminous red giant, it is not surprising that V399 Aur is a long-period variable. ET Tau is a fully analyzed eclipsing binary (EB), where Williamon et al. (2016) report parameters of $M_1 \simeq 14.3$, $T_1 \simeq 30\,300$ K, $L_1 = 30\,500 L_\odot$, and $M_2 = 6.3 \, \mathrm{M_\odot}$, $T_2 = 15\,000$ K and $L_2 = 6400 L_\odot$, respectively. This mass for the primary is much higher than found here (5.8–8.9 $\mathrm{M_\odot}$), but the SED also clearly rules out the high temperature and luminosity of the Williamon et al. (2016) model. In particular, the SED clearly breaks going into the UV rather than continuing the Rayleigh–Jeans rise that would be expected for 30000-K star.

Aside from HD 37424, all of the stars for which the age is constrained (i.e. excluding stars like HD 247176) favour ages $\log t \gtrsim 7.0$, and most are closer to $\log t = 7.5$. There are clearly a number of stars that have masses $> 10 \, \mathrm{M_\odot}$, so it seems likely that the progenitor of PSR J0538+2817 had an initial mass between $\simeq 13 \, \mathrm{M_\odot}$, since there are many remaining stars in this mass/age range, and $19 \, \mathrm{M_\odot}$ since all the stars appear to be older than $\log t = 7$. Dinçel et al. (2015) argued for a mass range of $13 \, \mathrm{M_\odot}$, their estimate of the mass of HD 37424 based on the spectral type, up to $25 \, \mathrm{M_\odot}$ based on the absence of nearby O stars. Note that we are not using HD 37424 in setting this limit because we will next argue that the system must have been a mass transfer binary.

We would like to determine the properties of the pre-SN binary to constrain both the size of the orbit and the mass of the progenitor.

Table 7. Luminous stars near HD 37424 and PSR J0538+2817.

Star	χ^2/N_{dof}	$\log(T_*/\mathrm{K})$	$\log(L_*/L_\odot))$	$M_*/M_\odot$	$\log t$	Comments
HD 39746	0.80	4.281 ± 0.040	4.761 ± 0.124	12.6–18.2	6.99–7.22	B1II
V1164 Tau	1.43	4.344 ± 0.050	4.524 ± 0.151	9.9–16.5	7.00–7.39	A, Ell
HD 38658	0.68	4.179 ± 0.033	4.424 ± 0.107	9.9–13.6	7.17–7.39	B3II
HD 36665	1.02	4.324 ± 0.052	4.379 ± 0.163	8.8–14.9	7.05–7.49	B1, Be star
HD 38017A	0.84	4.258 ± 0.027	4.289 ± 0.066	9.7–11.6	7.28–7.42	B3V, visual binary
HD 37424	0.89	4.431 ± 0.044	4.219 ± 0.128	10.1–15.4	<7.38	B9
HD 35347	1.61	4.220 ± 0.032	3.837 ± 0.081	7.0–8.7	7.49–7.69	B1V, Be star
ET Tau	1.22	4.160 ± 0.050	3.819 ± 0.160	6.2–9.4	7.44–7.81	B8, EB
HD 246821	0.84	3.886 ± 0.043	3.715 ± 0.142	5.8–8.9	7.48–7.90	F0
HD 248666	0.82	4.172 ± 0.057	3.708 ± 0.167	5.7–8.8	7.50–7.89	B
HD 38749	0.75	3.897 ± 0.023	3.599 ± 0.072	6.1–7.4	7.64–7.85	A5
HD 247176	0.29	4.216 ± 0.070	3.536 ± 0.204	4.9–8.5	6.69–8.04	B2V
HD 244610	1.46	4.076 ± 0.073	3.427 ± 0.197	4.6–7.5	7.63–8.12	B1V, Be star
TIC 3219130	0.91	3.528 ± 0.002	3.337 ± 0.014	0.6–2.7	8.84–9.99	M5
HD 246370	0.17	3.831 ± 0.022	3.314 ± 0.068	5.3–6.3	7.79–7.96	G5
TIC 76026324	1.20	3.587 ± 0.005	3.295 ± 0.013	1.6–5.6	7.91–9.37	M2/3
HD 245247	0.81	3.816 ± 0.012	3.073 ± 0.026	4.7–5.3	7.97–8.09	A7
V399 Aur	1.79	3.529 ± 0.002	2.856 ± 0.016	0.7–1.3	9.66–9.99	M2/3, LPV

Unfortunately, the geometry of the positions and proper motions can at best set a minimum projected size for the binary. The first problem is simply that parallaxes provide no useful information for constraining the line of sight separation at the time of the SNe. Then, in projection, it is only possible to rule out small separations but not to prove them. A solution with an explosion at a projected separation of zero is allowed if there is a reasonable probability that the cross-product of the present-day separation and proper motion differences can be zero. This is true for HD 37424, although it need not be so. However, the raw probability of a given minimum projected separation $R_\perp$ is just proportional to $R_\perp$ because given a random choice for $R_\perp$ a value close to zero is unlikely. A Bayesian corrects for this by using logarithmic prior of $1/R_\perp$, leading to a probability distribution, which is independent of $R_\perp$ when it is small. For sufficiently large $R_\perp$ ($\sim 30\,000$ AU for HD 37 424), the distribution cuts off because large projected separations are unlikely. It is, after all, how the star was selected. However, while we select based on the minimum projected separation, the explosion need not happen at this closest approach distance, so a larger separation cannot be ruled out. In sum, the positions and proper motions would allow the progenitor system to be anything from a contact binary to a very, very wide binary.

It is really the velocity of the star that constrains the orbit, which is why Dinçel et al. (2015) focus on the projected velocity of the star. They estimate a rest-frame proper motion of (10.0 ± 0.8, -5.9 ± 0.6) mas yr^{-1} after correcting for Galactic rotation and Solar motion using a model. For the Gaia EDR3 parallax distance of 1.5 kpc, this corresponds to 87 ± 9 km s^{-1}. They also measured an average heliocentric radial velocity of -8.9 ± 3.0 km s^{-1}. This implies an orbital separation smaller than the radius of a massive red supergiant, so Dinçel et al. (2015) suggest that the progenitor was a naked helium star with a mass as low as $2\,M_\odot$.

With *Gaia*, we can use the proper motions and radial velocities of nearby stars to define the local standard of rest. We selected stars in the same parallax range used for the luminous stars, a larger angular separation ($10°$), and apparent magnitudes within 1.5 mag of HD 37424 since kinematics depend on mass/luminosity. This yielded 523 stars with proper motions and 345 with radial velocities. HD 37424 does not have a *Gaia* radial velocity. These stars had a median proper motion of (0.78, -3.3) mas yr^{-1} with a dispersion

(estimated from the central 68 per cent of the sorted proper motions) of (1.9, 2.4) mas yr^{-1}, and a median radial velocity of 0.1 km s^{-1} with a dispersion of 29.8 km s^{-1}. Note that the intrinsic dispersions are more important than the typical measurement uncertainties. Subtracting this from the proper motion of HD 37424 implies an SN local rest-frame proper motion of (11.5, -6.1) mas yr^{-1} with uncertainties set by the local proper motion dispersion, or 94 ± 15 km s^{-1}. Similarly, subtracting the mean local RV from the Dinçel et al. (2015) velocity for HD 37424 gives a local rest-frame radial velocity of -9.0 ± 30.0 km s^{-1}.

The star has a small radial velocity compared to the velocities in the plane of the sky, and there are two arguments that the same is true of the present neutron star motions. First, Ng et al. (2007) argue that the pulsar wind nebula is seen almost edge on and aligned nearly perpendicular to the proper motion. Secondly, Yao et al. (2021) use scintillation of the pulsar signals off the near side of the SNR to estimate its distance from the neutron star and argue that the estimated distance puts the neutron star close to the centre of the SNR and so implies that it has a low line-of-sight velocity. For the neutron star, this could be entirely due to the kick, but it seems contrived to have the kick nearly cancel the motions along the line of sight. So for the present discussion, we assume that the pre-supernova binary effectively lay in the plane of the sky and that the orbit was circular.

Under these assumptions, the velocity of the star in the plane of the sky is

$$\vec{v}_* = v_o \frac{M_p}{M_T} \begin{pmatrix} \cos\theta \\ \sin\theta \end{pmatrix} \tag{14}$$

and the velocity of the neutron star is

$$\vec{v}_{NS} = -v_o \frac{M_*}{M_T} \begin{pmatrix} \cos\theta \\ \sin\theta \end{pmatrix} + v_k \begin{pmatrix} \cos\psi \\ \sin\psi \end{pmatrix}, \tag{15}$$

where M_* is the mass of HD 37424, M_p is the mass of the SN progenitor at death, $M_T = M_* + M_p$ is the total mass, $v_0 = (GM_T/a)^{1/2}$, where a is the semimajor axis, v_k is the neutron star kick velocity, and θ and ψ are the direction of the stellar velocity and the kick, respectively. As a function of the two masses, the proper motions and the estimated local standard of rest combine to give estimates of a, v_k, θ, and ψ.
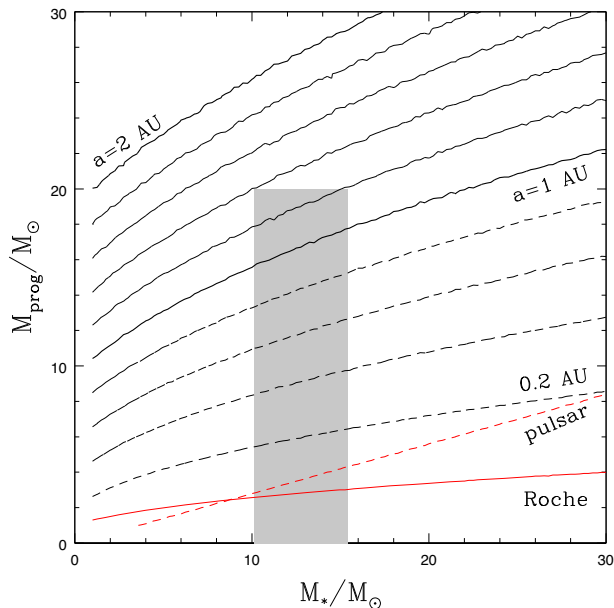
Figure 2. Semimajor axes as a function of the mass of HD 37424 (M_*) and the mass of the SN progenitor at the time of explosion (M_p). The shaded grey region is allowed by the fits to the SED of HD 37424 and the ages of nearby massive stars for the progenitor. Below the red Roche line, HD 37424 would fill its Roche lobe, and below the red dashed pulsar line the neutron star kick amplitude and direction become improbable. The kinematic uncertainties allow a 35 per cent dispersion in the semimajor axis at fixed mass. There is a narrow band of acceptable pulsar solutions below the Roche line, which has been excluded for clarity.
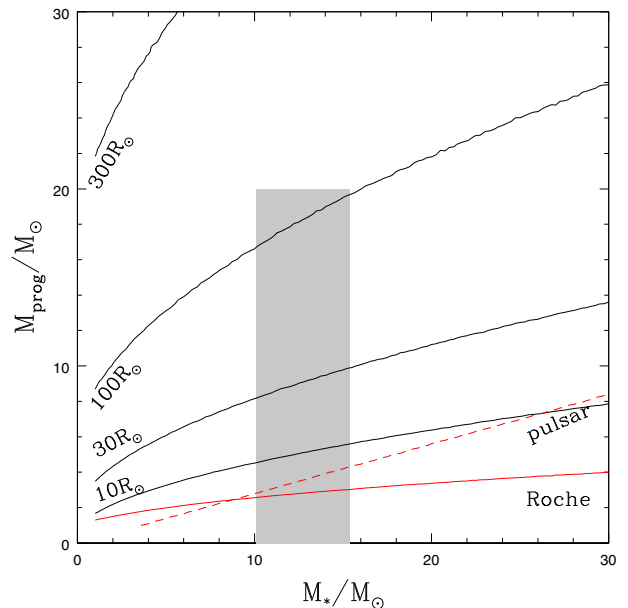
Figure 3. The Roche limit on the SN progenitor (black contours) over the same mass range as in Fig. 2 and with the same limits from the Roche radius of HD 37424 and the pulsar kinematics. The Roche limit on the progenitor is much smaller than the radii of red supergiants. The most likely scenario was that the progenitor was Roche lobe filling, transferring mass that 'rejuvenated' HD 37424 to make it appear younger than other nearby massive stars and then leading to a Type IIL or IIb supernova. While not drawn, a $3R_\odot$ Roche radius for the SN progenitor closely tracks the Roche radius limit for HD 37424.

We have several additional constraints on these parameters. First, from the SED models we have an estimate of M_*. Secondly, the pulsar spin axis, generally believed to be perpendicular to the wind nebula, is nearly perpendicular to the proper motion of the pulsar at a PA of $\theta_{\rm spin} = -11°$ or $12°$ off the neutron star velocity vector (Ng et al. 2007). This alignment is common and Ng & Romani (2007) use the distribution of misalignments to try to constrain the origin of neutron star kicks. If we model the misalignments reported by Ng & Romani (2007) with a Gaussian distribution corrected for the individual uncertainties, we find a best-fitting dispersion of $\sigma_\psi = 17°$. So, we can constrain the angle ψ as a position angle to be within σ_ψ of $\theta_{\rm spin}$. Thirdly, there are constraints on the amplitudes of neutron star kick velocities, where we use the estimate that the distribution of 1D coordinate velocities can be modelled as a Gaussian with a dispersion of $\sigma_k = 265\,\mathrm{km\,s^{-1}}$ (Hobbs et al. 2005). The results were almost identical if we instead used the two-Gaussian (slow and fast) kick model of Arzoumanian, Chernoff & Cordes (2002). Finally, we also have an estimate of the radius of HD 37424 from the SED models and can eliminate mass ranges where the Roche radius is smaller than the stellar radius, where we use the approximation for the mean Roche radius of Eggleton (1983).

Fig. 2 summarizes the results in the plane of the mass of HD 37424, M_*, and the mass of the progenitor at death, M_p. A broader than plausible mass range is shown for both, with a grey shaded region giving the SED-based mass estimates for HD 37424 and a generous upper limit of $M_p < 20\,\mathrm{M_\odot}$ based on the properties of the surrounding stars. Contours show the semimajor axis of the orbit implied by the masses and kinematics. For a given mass, the uncertainties in the kinematics produce a dispersion of $\simeq 35$ per cent around this central value across the plane of masses. For progenitor masses below the line labelled

'Roche', HD 37424 would be overflowing its Roche lobe, given its radius of $(5.9 \pm 0.3)R_\odot$. For progenitor masses below the line labelled 'pulsar,' the neutron star properties (kick and alignment) are unlikely. Over the rest of the plane, both the implied kick velocity and its alignment relative to the spin are consistent with expectations. There is a narrow band below the Roche curve where the pulsar kick velocity and direction are again consistent with expectations that we have suppressed for clarity.

In terms of the orbital kinematics, production of a neutron star in a supernova and the properties of the neutron star kick, there is a broad progenitor mass range leading to reasonable solutions. The problem, already noted by Dinçel et al. (2015), is that a 10–20 $\mathrm{M_\odot}$ red supergiant should be significantly larger than these semimajor axes. Groh et al. (2013) find $547R_\odot = 2.5$ AU ($931R_\odot = 4.3$ AU) for an initial mass of $10\,\mathrm{M_\odot}$ ($20\,\mathrm{M_\odot}$) and Sukhbold et al. (2016) have $414R_\odot = 1.9$ AU ($1065R_\odot = 5.0$ AU). This problem cannot be solved by inclining the orbit out of the plane of the sky. Fig. 3 illustrates this problem with contours for the Roche limit of the progenitor. Dinçel et al. (2015) argue that the progenitor may have been a naked helium star at death, but this pushes into the very low pre-SN progenitor mass range where there are problems with the pulsar kinematics and the Roche limit of HD 37424.

The simplest solution is that the system was likely an interacting binary at death, with a Roche lobe-filling progenitor transferring mass to HD 37424. The mass transfer would help to explain why HD 37424 appears anomalously young and hot compared to the other stars in the field. The Roche limit is sufficiently small that the progenitor would have lost much of its hydrogen leading to a Type IIL or IIb supernova. In combination, these two classes represent ~ 16 per cent of ccSNe (Smith et al. 2011; Eldridge et al. 2013), so it is not a particularly improbable scenario for a randomly selected case.

Table 8. Constraints on binaries.

Case	Non-interacting incomplete		Non-interacting complete	
	Median	90% confidence	Median	90% confidence
Not binary at death	72.0%	52.2%–86.4%	76.0%	56.0%–89.2%
Bound binary	13.9%	5.4%–27.2%	9.5%	3.6%–19.7%
Interacting binary	10.2%	3.2%–22.3%	5.8%	1.8%–13.1%
Non-interacting binary		<8.5%		<8.9%
Unbound binary	12.5%	2.8%–31.3%	13.2%	3.0%–32.8%

6 DISCUSSION

We searched for unbound stellar companions to seven non-binary neutron stars, two binary neutron stars, and one binary black hole system that are both associated with SNRs and have proper motions. We identify only one convincing candidate, HD 37424 in G180.0−01.7, which was originally identified by Dinçel et al. (2015) and also confirmed using different methods by Boubert et al. (2017). All the remaining candidates are lower mass and have high probabilities of being false positives. The mass limit to which companions can be ruled out depends on the SNR, but a conservative limit is that there are no unbound binary or triple systems other than HD 37424 with masses $\gtrsim 5\,M_\odot$.

We estimate that HD 37424 has a mass of 10–$15\,M_\odot$ and that it was probably in a mass transfer binary with a semimajor axis of ~ 1 AU that would partly strip the neutron star progenitor and lead to a Type IIL or IIb SN. The progenitor was likely a 13–$19\,M_\odot$ star at birth based on the properties of the stars within 100 pc of the explosion. These conclusions agree with Dinçel et al. (2015) except for the nature of the progenitor at death, where Dinçel et al. (2015) suggest that it was a fully stripped helium star.

By combining this work, Kochanek (2018), and Kochanek et al. (2019), we can constrain all of the possibilities for the binary properties and outcomes of explosions producing neutron stars. In Kochanek (2018), we showed that the Crab, Cas A, and SN 1987A were not binaries at the time of explosion. Because these SNRs are so young, there is no need for proper motion information. We are assuming that SN 1987 A produced a neutron star (see e.g. Cigan et al. 2019; Greco et al. 2021). In Kochanek et al. (2019), we searched for surviving binaries starting from an initial sample of 49 SNRS. Of these, 23 contained compact objects where it was practical to carry out a search, and this included three previously identified HMXBs. If we drop SS 433 as a black hole system, then there were two interacting binaries and no non-interacting binaries in a sample of 22 explosions producing neutron stars.

We can combine all of these results to jointly estimate the fraction $f_n = 1 - f_u - f_b$ of SN producing neutron stars that are not binaries at the time of the SN, the fraction f_u leading to binaries that are unbound after the explosion, and the faction $f_b = f_i + f_p$ leading to binaries that are bound, where fraction f_i produces interacting binaries and f_p produces non-interacting (passive) binaries. The multinomial probability distribution is

$$f_n^9 (1 - f_b)^{11} f_u f_i^2 \qquad (16)$$

since we have nine SNR containing neither bound nor unbound binaries, 11 that contain no bound binary but could be unbound binaries, one unbound binary, and two interacting binaries. Again, we conservatively mean stellar companions $\gtrsim 5\,M_\odot$, although the mass limits for individual systems can be significantly tighter. This case, 'Non-Interacting Incomplete' in Table 8, assumes that the presence of the interacting companion does not bias whether the interacting

binary was included in the sample of 23 SNRs where Kochanek et al. (2019) searched for bound companions. Using uniform priors for the fractions, the probability can be marginalized to obtain the probability distribution for each of these fractions, with the median values and 90 per cent confidence ranges given in Table 8.

On the other hand, the 23 SNRs analyzed by Kochanek et al. (2019) may include all interacting binaries in the parent sample of 49 SNRs because their additional X-ray, γ-ray, or radio emission makes them trivial to detect. If so, we have overestimated the probability of producing an interacting binary. If we assume that all interacting binaries were included (case 'Non-Interacting Complete'), then there were two interacting neutron star binaries in a sample of 43 SNRs after making a rough correction for contamination by Type Ia SN (see Kochanek et al. 2019). In this case, the multinomial probability distribution becomes

$$f_n^9 (1 - f_b)^{11} (1 - f_i)^{20} f_u f_i^2 \qquad (17)$$

because there are an additional 20 SNRs known not to contain interacting binaries. The results for this case are also given in Table 8 and the true answer should be bounded by these two limits.

We will not attempt a similarly complete sub-division into cases for the question of triple systems at death in part because we lack information on whether the interacting binaries and HD 37424 have distant bound companions. However, of the 10 systems where the compact object is not in a binary (the seven here plus the Crab, Cas A, and SN 1987A), none are fully unbound triples. So of SN that do not leave bound binaries, less than 18.9 per cent can be fully unbound massive star triples. Of the three systems that are interacting binaries, none is a partially unbound triple. Thus, of SN leaving interacting binaries, <43.7 per cent can have an unbound triple companion. Note that these are fractions of systems that are not binaries or binaries after the explosion, while the statistics for binaries in Table 8 are all as fractions of SN.

While there will be a point where systematic problems due to any correlation between the detectable life times of SNRs and any of the binary properties we consider will become important, statistical uncertainties are likely dominant at present (see the discussion in Kochanek et al. 2019). It certainly seems possible to significantly improve the statistics simply by identifying more compact objects in SNRs with reasonable distances and extinctions and then measuring their proper motions. In Kochanek et al. (2019), we found that the problem for many of the SNRs that could be studied was that there were multiple, faint, X-ray sources superposed on the remnant. Detecting a proper motion would clearly separate the neutron star from the contaminating background sources. Where the neutron star is already detected, a sufficient amount of time has likely passed since the original observations that proper motions can be measured or at least tightly restricted. Simply knowing that the neutron star has (say) moved less than $0\rlap{.}''1$ in 20 yr restricts the allowed position 10^4 yr ago to under an arcminute.

The biggest cause of false positives in searching for unbound stars is the lack of good distances to the SNRs. In theory, this can be addressed by searching for absorption features associated with the SNR in the spectra of superposed stars. This approach appears to have worked quite well for the Vela SNR, where the estimated distance of 250 ± 30 pc by Cha, Sembach & Danks (1999) based on the appearance of high-velocity components in the Na D and Ca II absorption lines of more distant stars agrees almost exactly with the Dodson et al. (2003) pulsar parallax distance ($\varpi^{-1} = 286 \pm 16$ pc). The absorption lines of the background stars to Vela are also unusual because many of them are significantly time variable (see Kameswara Rao et al. 2020 most recently). With *Gaia* distances and fibre-fed Echelle spectrographs, this would appear to be a straightforward approach to measuring the distances to many SNRs.

Improving the constraints on fully unbound triples is much easier than doing so for unbound binaries because accurate distances to the SNR and pulsar proper motions are less needed for the control of false positives. Particularly, if restricted to relatively massive and rare stars (say $>5\,M_\odot$), the requirement that two stars with *Gaia* proper motions and parallaxes have consistent distances and paths that intersect near the centre of the SNR at some point in the last 10^5 yr will greatly suppress or eliminate false positives. The same is also true for a partly unbound binary where the compact object is in a binary because *Gaia* supplies the parallax and proper motion of the binary companion to the compact object.

HD 37424 is a very convincing case of an unbound binary companion, but what can be done both to strengthen the evidence and use it to learn something about binary evolution, SN, and SN in binaries? Dinçel et al. (2015) looked for high-velocity absorption features in their Echelle spectra of HD 37424 and found nothing but note that the signal-to-noise ratio of the spectrum was relatively low. Finding such features would help to confirm the hypothesis and it would be trivial to obtain far lower noise spectra from the ground. It might be better, however, to look in the UV with *HST* where there are many more lines (see e.g. the study of the SN 1006 SNR by Winkler et al. 2005). An unusually fast rotation rate would help to confirm the interacting binary scenario, but a low estimate of $v \sin i$ will be difficult to interpret, given the evidence that the binary likely lay in the plane of the sky. The supernova shock wave affects the structure of the outer layers and the luminosity of the star, but any time evolution from the relaxation back to steady state is likely impossible to detect with the passage of 30 000 yr (see e.g. Ogata, Hirai & Hijikawa 2021). The best route may be to look for abundance anomalies, as several HMXBs are known to have anomalous α-element abundances presumably due to capturing some of the ejecta from the SN (e.g. Israelian et al. 1999, Orosz et al. 2001).

DATA AVAILABILITY STATEMENT

All data used in this paper are publicly available.

REFERENCES

Abbott R. et al., 2021, ApJ, 913, L7
Anderson S. B., Cadwell B. J., Jacoby B. A., Wolszczan A., Foster R. S., Kramer M., 1996, ApJ, 468, L55
Antonini F., Toonen S., Hamers A. S., 2017, ApJ, 841, 77
Arzoumanian Z., Chernoff D. F., Cordes J. M., 2002, ApJ, 568, 289
Aschenbach B., Egger R., Trümper J., 1995, Nature, 373, 587
Belczynski K., Kalogera V., Bulik T., 2002, ApJ, 572, 407
Belczynski K., Kalogera V., Rasio F. A., Taam R. E., Zezas A., Bulik T., Maccarone T. J., Ivanova N., 2008, ApJS, 174, 223
Benvenuto O. G., Bersten M. C., Nomoto K., 2013, ApJ, 762, 74
Bietenholz M. F., 2006, ApJ, 645, 1180
Bietenholz M. F., Kondratiev V., Ransom S., Slane P., Bartel N., Buchner S., 2013, MNRAS, 431, 2590
Blundell K. M., Bowler M. G., 2004, ApJ, 616, L159
Boubert D., Fraser M., Evans N. W., Green D. A., Izzard R. G., 2017, A&A, 606, A14
Bovy J., Rix H.-W., Green G. M., Schlafly E. F., Finkbeiner D. P., 2016, ApJ, 818, 130
Bressan A., Marigo P., Girardi L., Salasnich B., Dal Cero C., Rubele S., Nanni A., 2012, MNRAS, 427, 127
Camilo F. et al., 2001, ApJ, 557, L51
Camilo F. et al., 2002, ApJ, 571, L41
Castelli F., Kurucz R. L., 2003, Modelling Stellar Atmos., 210, 20P
Cha A. N., Sembach K. R., Danks A. C., 1999, ApJ, 515, L25
Chatterjee S. et al., 2009, ApJ, 698, 250
Cigan P. et al., 2019, ApJ, 886, 51
Clark D. H., Stephenson F. R., 1977, Oxford [Eng.], 1st edn. Pergamon Press, New York
Corbet R. H. D. et al., 2011, Astron. Telegram, 3221
Cutri R. M. et al., 2012, VizieR Online Data Catalog, II/311
de Luca A., Mereghetti S., Caraveo P. A., Moroni M., Mignani R. P., Bignami G. F., 2004, A&A, 418, 625
Dinçel B., Neuhäuser R., Yerli S. K., Ankay A., Tetzlaff N., Torres G., Mugrauer M., 2015, MNRAS, 448, 3196
Dodson R., Legge D., Reynolds J. E., McCulloch P. M., 2003, ApJ, 596, 1137
Dominik M., Belczynski K., Fryer C., Holz D. E., Berti E., Bulik T., Mandel I., O'Shaughnessy R., 2013, ApJ, 779, 72
Drimmel R., Cabrera-Lavers A., López-Corredoira M., 2003, A&A, 409, 205
Dubus G., 2013, A&ARv, 21, 64
Eggleton P. P., 1983, ApJ, 268, 368
Eldridge J. J., Fraser M., Smartt S. J., Maund J. R., Crockett R. M., 2013, MNRAS, 436, 774
Eldridge J. J. et al., 2017, PASA, 34, e058
Fragione G., Kocsis B., 2019, MNRAS, 486, 4781
Fraser M., Boubert D., 2019, ApJ, 871, 92
Fruchter A. S., Taylor J. H., Backer D. C., Clifton T. R., Foster R. S., 1988, Nature, 331, 53
Gaia Collaboration 2016, A&A, 595, A1
Gaia Collaboration 2021, A&A, 649, A1
Giacani E. B., Dubner G. M., Green A. J., Goss W. M., Gaensler B. M., 2000, AJ, 119, 281
Gotthelf E. V., Halpern J. P., 2009, ApJ, 695, L35
Gotthelf E. V., Helfand D. J., Newburgh L., 2007, ApJ, 654, 267
Greco E. et al., 2021, ApJ, 908, L45
Green D. A., 2014, Bull. Astron. Soc. India, 42, 47
Green D. A., 2019, JA&A, 40, 36
Green G. M., Schlafly E., Zucker C., Speagle J. S., Finkbeiner D., 2019, ApJ, 887, 93
Gregory P. C., Fahlman G. G., 1980, Nature, 287, 805
Groh J. H., Meynet G., Georgy C., Ekström S., 2013, A&A, 558, A131
Guseinov O. H., Ankay A., Tagieva S. O., 2005, Astrophysics, 48, 330

Gustafsson B., Edvardsson B., Eriksson K., Jørgensen U. G., Nordlund A., Plez B., 2008, A&A, 486, 951

Halpern J. P., Gotthelf E. V., 2015, ApJ, 812, 61

Hamers A. S., Rantala A., Neunteufel P., Preece H., Vynatheya P., 2021, MNRAS, 502, 4479

Han Z.-W., Ge H.-W., Chen X.-F., Chen H.-L., 2020, Res. Astron. Astrophys., 20, 161

Henden A. A., Templeton M., Terrell D., et al., 2016, Vizier online data catalog, II/336

Hillwig T. C., Gies D. R., 2008, ApJ, 676, L37

Hinton J. A. et al., 2009, ApJ, 690, L101

Hobbs G., Lorimer D. R., Lyne A. G., Kramer M., 2005, MNRAS, 360, 974

Hoffleit D., Warren W. H., 1995, VizieR Online Data Catalog, V/50x

Hohle M. M., Neuhäuser R., Schutz B. F., 2010, Astron. Nachr., 331, 349

Hui C. Y., Becker W., 2006, A&A, 454, 543

Israelian G., Rebolo R., Basri G., Casares J., Martín E. L., 1999, Nature, 401, 142

Jayasinghe T. et al., 2021, MNRAS, 504, 2577

Kalogera V., Belczynski K., Kim C., O'Shaughnessy R., Willems B., 2007, Phys. Rep., 442, 75

Kameswara Rao N., Lambert D. L., Reddy A. B. S., Gupta R., Muneer S., Varghese B., Singh H. P., 2020, MNRAS, 493, 497

Kerzendorf W. E. et al., 2019, A&A, 623, A34

Kobulnicky H. A., Fryer C. L., 2007, ApJ, 670, 747

Kochanek C. S., 2014, ApJ, 785, 28

Kochanek C. S., 2018, MNRAS, 473, 1633

Kochanek C. S., Auchettl K., Belczynski K., 2019, MNRAS, 485, 5394

Koo B.-C., Reach W. T., Heiles C., Fesen R. A., Shull J. M., 1990, ApJ, 364, 178

Koo B.-C., Yun M.-S., Ho P. T. P., Lee Y., 1993, ApJ, 417, 196

Kothes R., Foster T., 2012, ApJ, 746, L4

Kothes R., Fedotov K., Foster T. J., Uyanıker B., 2006, A&A, 457, 1081

Kramer M., Lyne A. G., Hobbs G., Löhmer O., Carr P., Jordan C., Wolszczan A., 2003, ApJ, 593, L31

Krause O., Birkmann S. M., Usuda T., Hattori T., Goto M., Rieke G. H., Misselt K. A., 2008, Science, 320, 1195

Kulkarni S. R., Clifton T. C., Backer D. C., Foster R. S., Fruchter A. S., 1988, Nature, 331, 50

Lam C. Y., Lu J. R., Hosek M. W., Dawson W. A., Golovich N. R., 2020, ApJ, 889, 31

Large M. I., Vaughan A. E., Mills B. Y., 1968, Nature, 220, 340

Leahy D. A., Ranasinghe S., 2012, MNRAS, 423, 718

Lewandowski W., Wolszczan A., Feiler G., Konacki M., Sołtysiński T., 2004, ApJ, 600, 905

Livingstone M. A., Ransom S. M., Camilo F., Kaspi V. M., Lyne A. G., Kramer M., Stairs I. H., 2009, ApJ, 706, 1163

Lux O., Neuhäuser R., Mugrauer M., Bischoff R., 2021, Astron. Nachr., 342, 553

Margon B., 1984, ARA&A, 22, 507

Marigo P., Bressan A., Nanni A., Girardi L., Pumo M. L., 2013, MNRAS, 434, 488

Marshall D. J., Robin A. C., Reylé C., Schultheis M., Picaud S., 2006, A&A, 453, 635

Marshall H. L., Canizares C. R., Hillwig T., Mioduszewski A., Rupen M., Schulz N. S., Nowak M., Heinz S., 2013, ApJ, 775, 75

Mayer M. G. F., Becker W., 2021, A&A, 651, A40

Michalik D., Lindegren L., Hobbs D., 2015, A&A, 574, A115

Moe M., Di Stefano R., 2017, ApJS, 230, 15

Murray S. S., Slane P. O., Seward F. D., Ransom S. M., Gaensler B. M., 2002, ApJ, 568, 226

Ng C.-Y., Romani R. W., 2007, ApJ, 660, 1357

Ng C.-Y., Romani R. W., Brisken W. F., Chatterjee S., Kramer M., 2007, ApJ, 654, 487

Ogata M., Hirai R., Hijikawa K., 2021, MNRAS, 505, 2485

Orosz J. A. et al., 2001, ApJ, 555, 489

Panferov A. A., 2017, A&A, 599, A77

Pastorelli G. et al., 2020, MNRAS, 498, 3283

Patel S. K. et al., 2001, ApJ, 563, L45

Pavlov G. G., Zavlin V. E., Sanwal D., Burwitz V., Garmire G. P., 2001a, ApJ, 552, L129

Pejcha O., Thompson T. A., 2015, ApJ, 801, 90

Perryman M. A. C. et al., 1997, A&A, 500, 501

Podsiadlowski P., 1992, PASP, 104, 717

Renzo M. et al., 2019, A&A, 624, A66

Rest A. et al., 2011, ApJ, 732, 3

Reynolds S. P., Aller H. D., 1988, ApJ, 327, 845

Reynoso E. M., Green A. J., Johnston S., Dubner G. M., Giacani E. B., Goss W. M., 2003, MNRAS, 345, 671

Reynoso E. M., Cichowolski S., Walsh A. J., 2017, MNRAS, 464, 3029

Roberts D. A., Goss W. M., Kalberla P. M. W., Herbstmeier U., Schwarz U. J., 1993, A&A, 274, 427

Roger R. S., Milne D. K., Kesteven M. J., Wellington K. J., Haynes R. F., 1988, ApJ, 332, 940

Ruiz M. T., May J., 1986, ApJ, 309, 667

Sana H. et al., 2012, Science, 337, 444

Sánchez-Cruces M., Rosado M., Fuentes-Carrera I., Ambrocio-Cruz P., 2018, MNRAS, 473, 1705

Skrutskie M. F. et al., 2006, AJ, 131, 1163

Slane P., Helfand D. J., van der Swaluw E., Murray S. S., 2004, ApJ, 616, 403

Smith N., Li W., Filippenko A. V., Chornock R., 2011, MNRAS, 412, 1522

Sofue Y., Furst E., Hirth W., 1980, PASJ, 32, 1

Strader J., Chomiuk L., Cheung C. C., Salinas R., Peacock M., 2015, ApJ, 813, L26

Sukhbold T., Ertl T., Woosley S. E., Brown J. M., Janka H.-T., 2016, ApJ, 821, 38

Taylor J. H., Manchester R. N., Lyne A. G., 1993, ApJS, 88, 529

Tendulkar S. P., Cameron P. B., Kulkarni S. R., 2013, ApJ, 772, 31

Thompson G. I. et al., 1978, a compilation of absolute stellar fluxes measured by the sky survey telescope (S2/68) aboard the ESRO satellite TD-1

Thompson T. A. et al., 2019, Science, 366, 637

Toonen S., Portegies Zwart S., Hamers A. S., Bandopadhyay D., 2020, A&A, 640, A16

van den Bergh S., 1980, JA&A, 1, 67

van Leeuwen F., 2007, A&A, 474, 653

Verbiest J. P. W., Weisberg J. M., Chael A. A., Lee K. J., Lorimer D. R., 2012, ApJ, 755, 39

Villaseñor J. I. et al., 2021, MNRAS, preprint (arXiv:2107.10170)

Waisberg I. R., Romani R. W., 2015, ApJ, 805, 18

Welsh B. Y., Sfeir D. M., Sallmen S., Lallement R., 2001, A&A, 372, 516

Wenger M. et al., 2000, A&AS, 143, 9

Williamon R. M. et al., 2016, PASP, 128, 124202

Winkler P. F., Tuttle J. H., Kirshner R. P., Irwin M. J., in Roger R. S., Landecker T. L., eds, 1988, IAU Colloq. 101: Supernova Remnants and the Interstellar Medium, Cambridge Unive Press, p. 65

Winkler P. F., Long K. S., Hamilton A. J. S., Fesen R. A., 2005, ApJ, 624, 189

Yao J. et al., 2021, Nature Astron., 5, 78

Zacharias N. et al., 2005, VizieR Online Data Catalog, I/297

Zavlin V. E., Pavlov G. G., Sanwal D., Trümper J., 2000, ApJ, 540, L25

Zeiger B. R., Brisken W. F., Chatterjee S., Goss W. M., 2008, ApJ, 674, 271

APPENDIX A: SAMPLE

We examined 10 SNRs where there is a proper motion measurement either for the neutron star (seven systems) or its binary companion (three systems) that also have distances and extinctions small enough to search for stellar companions using Gaia EDR3 parallaxes and proper motions. For statistical analyses, we also include the Crab (G184.6−05.8), Cas A (G117−02.1), and SN 1987A. Because these SNRs are very young, the plausible regions in which any former companion could lie are so small that Kochanek (2018) (also see Fraser & Boubert 2019; Kerzendorf et al. 2019) could demonstrate

that there were no bound or unbound former companions down to mass ratios $\lesssim 0.1$ even in the absence of proper motion data.

A1 G039.7−02.0

Contains the interacting compact object binary SS 433 (for a review, see Margon 1984). We use the position and size of the SNR from Green (2019). SS 433 is more distant ($\varpi^{-1} = 8.5$ kpc) and highly extincted [`mwdust` $E(B - V) \sim 1$–2 mag] than the other SNRs we consider here, so we selected stars to $G < 20$ mag instead of $G < 18$ mag. Even so, this means that we are really sensitive to stars only in the $M > 5\,\mathrm{M}_\odot$ bin. To limit the number of stars given the faint magnitude limit, we considered stars only with $0 < \varpi \leq 0.25$ mas, corresponding to the $\sim$5-σ range of the Gaia EDR3 parallax. The distance implied by the Gaia EDR3 parallax (6.1–13.9 kpc at 2σ) significantly disagrees with distance estimates from kinematic models of the SS 433 jets (5.5 ± 0.2, Blundell & Bowler 2004; 4.5 ± 0.2 kpc, Marshall et al. 2013) but the parallax $RUWE =$ 1.24 is not anomalously high. As a precaution, we also searched for unbound stars using a parallax of 0.208 ± 0.042 mas, which encompasses the kinematic distance estimates and again found no candidates. The age of the remnant is estimated to be anywhere from 10^4 to 10^5 yr (see e.g. Panferov 2017).

A2 G069.0+02.7 (CTB 80)

Contains the radio pulsar PSR B1951+32 (Kulkarni et al. 1988), which has a proper motion of $(-28.8 \pm 0.9, -14.7 \pm 0.9)$ mas yr^{-1} (Zeiger et al. 2008). There is no parallax for the pulsar. Koo et al. (1993) roughly estimate the distance to CTB 80 to be $d \simeq 2$ kpc, while Leahy & Ranasinghe (2012) estimate a distance of $1.5^{+0.6}_{-0.4}$ kpc. Kulkarni et al. (1988) estimate 1.4 kpc from the dispersion measure to the pulsar. We adopt a loose limit on the 'parallax' of the SNR of $\varpi = 0.75 \pm 0.25$ mas, which encompasses 1–2 kpc at 1σ. We adopt 19:54:50 33:00:30 for the centre of the SNR from Zeiger et al. (2008), and a diameter of 80 arcmin from Green (2014). The pulsar has a spin-down age of $\tau_c = P/2\dot{P} = 107\,000$ yr (Fruchter et al. 1988). Koo et al. (1990) estimate an age from the size and expansion velocity of the SNR of $77\,000$ yr for a distance of 2 kpc. For a limiting magnitude of $G < 18$ mag, the sample of $\sim\mathrm{M}_\odot$ stars will be incomplete, but the false-positive rate is also too high to search for such low-mass companions.

A3 G109.1−01.0

This SNR contains the anomalous X-ray pulsar 1E 2259+586 (Gregory & Fahlman 1980), which has a proper motion of $(-6.4 \pm 0.6, -2.3 \pm 0.6)$ mas yr^{-1} (Tendulkar, Cameron & Kulkarni 2013). Verbiest et al. (2012) estimate a distance of 4.1 ± 0.7 kpc. Kothes & Foster (2012) and Sánchez-Cruces et al. (2018) argue for a lower distance of 3.2 ± 0.2 kpc. We adopt a 'parallax' of $\varpi = 0.28 \pm 0.05$, which spans 3.2–4.3 kpc at 1σ. Kothes et al. (2006) derive a centre of 23:01:39+58:53:00 with a diameter of 33 arcmin. The spin-down age is $230\,000$ yr, but estimates based on the remnant are generally $10\,000$–$20\,000$ yr (see Sánchez-Cruces et al. 2018). $N(H) = (0.93 \pm 0.04) \times 10^{22}$ cm^2 (Patel et al. 2001), corresponding to $E(B - V) = 1.60 \pm 0.07$. For a limiting magnitude of $G < 18$ mag and a distance of 4 kpc, we can search for only $>4\,\mathrm{M}_\odot$ companions.

A4 G130.7+03.1 (3C 58, SN 1181)

This SNR contains the X-ray pulsar PSR J0205+6449 (Murray et al. 2002), which has a proper motion of $(-1.40 \pm 0.16, 0.54 \pm 0.58)$ mas yr^{-1} (Bietenholz et al. 2013). Roberts et al. (1993) estimate a kinematic (H I) distance of 3.2 kpc, while Camilo et al. (2002) obtain $4.5^{+1.6}_{-1.2}$ kpc based on the dispersion measure to the pulsar, and Kothes & Foster (2012) argue for 2 kpc. The age is also uncertain. The spin-down age is $5.4\,000$ yr (Livingstone et al. 2009) while it would only be $0.84\,000$ yr old if associated with SN 1181 (Clark & Stephenson 1977). Studies of the remnant (e.g. Bietenholz 2006) generally argue that the SNR must be several thousand years old. We adopt a 'parallax' of 0.36 ± 0.14 mas, which spans 2.0–4.7 kpc at 1σ. Gotthelf, Helfand & Newburgh (2007) propose 02:05:33.97 64:49:50 as the explosion centre[1] and the asymmetric remnant has an average diameter of approximately 8.1 arcmin (Reynolds & Aller 1988). Slane et al. (2004) find $N(H) = (4.5 \pm 0.1) \times 10^{21}$ cm^2, corresponding to $E(B - V) \simeq 0.77 \pm 0.02$. For a limiting magnitude of $G < 18$ mag and a distance of 5 kpc, we can search for only $>3\,\mathrm{M}_\odot$ companions.

A5 G180.0−01.7

This SNR contains the radio pulsar PSR J0538+2817 (Anderson et al. 1996). Ng et al. (2007) measured VLBI parallax and proper motions of $\varpi = 0.68 \pm 0.15$ mas and $(-23.53 \pm 0.16, 52.59 \pm 0.13)$ mas yr^{-1}, and Chatterjee et al. (2009) measured $\varpi = 0.72^{+0.12}_{-0.09}$ and $(-23.57 \pm 0.10, 52.87^{+0.09}_{-0.10})$ mas yr^{-1}. The Chatterjee et al. (2009) analysis appears to use the Ng et al. (2007) data but considers more sources of systematic error, so we use their values and the larger values for the asymmetric errors. Kramer et al. (2003) estimate that the centre of the SNR is at 05:40:01+27:48:09, and Dinçel et al. (2015) estimate that the diameter is 200 arcmin. Based on the disrupted binary, Dinçel et al. (2015) estimate an age of (30 ± 4) thousand years. The pulsar has a spin-down age of $620\,000$ yr (Lewandowski et al. 2004). Based on a Sedov model of the SNR, Sofue, Furst & Hirth (1980) estimated the age of the SNR as $200\,000$ yr for a distance of 1.6 kpc. Ng et al. (2007) also find $N(H) \simeq (2.7 \pm 0.3) \times 10^{21}$ cm^2, implying $E(B - V) \simeq 0.5 \pm 0.1$. Even at a higher distance of 1 kpc, we can search for companions down to $>1\,\mathrm{M}_\odot$.

Dinçel et al. (2015) and later Boubert et al. (2017) identify HD 37424 as a candidate disrupted binary companion. HD 37424 has a Gaia EDR3 parallax and proper motion of $\varpi = 0.654 \pm 0.028$ mas and $(12.229 \pm 0.036, -9.407 \pm 0.017)$ mas yr^{-1}. The parallaxes are mutually consistent to 0.5σ. Dinçel et al. (2015) were concerned that the stars HD 36665 and HD 37318 show absorption features due to the SNR but had distance estimates that placed them in the foreground. In Gaia EDR3, these stars have parallaxes of $\varpi = 0.702 \pm 0.031$ mas and $\varpi = 0.566 \pm 0.030$ mas, so statistically, HD 36665 could be more distant, and HD 37318 clearly is more distant than the SNR.

A6 205.5+00.5 (Monoceros loop)

The Monoceros loop is associated with the γ-ray source HESS J0632+057. The SNR was identified prior to the discovery of the γ-ray source. Hinton et al. (2009) also identified it as an X-ray source and suggested that it was in a binary with the massive star MWC 148. The high-energy emissions are believed to be

---

[1]The text of Gotthelf et al. (2007) gives the declination of the centre as 63:49:50, but this appears to be a misprint, given the figures and the discussion.

due to interactions between a pulsar and the stellar wind (see the review by Dubus 2013). We use the centre and size of the SNR from Green (2019). Boubert et al. (2017) identify HD 261393 as a candidate disrupted binary companion in this SNR but its parallax is inconsistent with that of MWC 148 (see text). Welsh et al. (2001) estimate an age of 30 000–150 000 yr.

A7 G260.4−03.4 (Puppis A)

Puppis A contains the X-ray pulsar PSR J0821−4300 (Gotthelf & Halpern 2009), where Mayer & Becker (2021) measure a proper motion of $(-74.2^{+7.4}_{-7.7}, -30.3^{+6.2}_{-6.2})$ mas yr^{-1}. We round the asymmetric uncertainties upwards. Reynoso, Cichowolski & Walsh (2017) estimate a kinematic distance to the SNR of 1.3 ± 0.3 kpc, although earlier estimates in Reynoso et al. (2003) were higher at 2.2 kpc. We adopt a 'parallax' of $\varpi = 0.75 \pm 025$ mas, which spans 1–2 kpc at 1σ. Winkler et al. (1988) found an explosion centre of 08:22:27.5−42:57:29 based on the proper motions of optical filaments in the SNR and Green (2014) gives a diameter of 60 arcmin. The motions of the optical filaments also imply an age of 3700 ± 300 yr (ignoring deceleration). Hui & Becker (2006) find $N(H) = (3.7 \pm 0.1) \times 10^{21}$ cm^2 corresponding to $E(B - V) = 0.63 \pm 0.02$. For $G < 18$ mag and a distance of 2 kpc, we can search for companions down to $>2\,M_{\odot}$.

A8 G263.9−03.3 (Vela)

The Vela pulsar (PSR J0835−4510, Large, Vaughan & Mills 1968) has a well-measured parallax ($\varpi = 3.5 \pm 0.2$) and proper motion $(-49.68 \pm 0.06, 29.9 \pm 0.1)$ mas yr^{-1} from Dodson et al. (2003). We could find no explicit estimate for the centre of the Vela SNR. Aschenbach, Egger & Trümper (1995) clearly made such an estimate, as they report that it is 25 ± 5 arcmin from the pulsar but do not include the actual coordinates. They report the diameter of the remnant as 8.3°. The position given by Green (2014) is visibly offset from the centre of the X-ray image of the SNR in Aschenbach et al.

(1995) and the reported diameter is only 4.3°. We set the centre of the SNR to be 25 arcmin backwards from the neutron star along its proper motion vector, which should be the Aschenbach et al. (1995) centre and use their larger diameter. Taylor, Manchester & Lyne (1993) give a spin-down age of 11 000 yr. Estimates based on the properties of the SNR by Aschenbach et al. (1995) range from 8000 to 37 000 yr. $N(H) = (3.0 \pm 0.3) \times 10^{20}$ cm^2 (Pavlov et al. 2001a). This column density implies $E(B - V) \simeq 0.05$ mag. With its proximity and low extinction, there is no problem searching for companions down to $>1\,M_{\odot}$.

A9 G284.3−01.8

This SNR is associated with the γ-ray source 1FGL J1018.6−5856, and it was identified as an HMXB by Corbet et al. (2011) with the star 2MASS J10185560−5856459. There is also an X-ray pulsar, PSR J1016−5857, on the edge or just outside the remnant (Camilo et al. 2001). Like HESS J0632+057, the high-energy emission is believed to be due to interactions between a pulsar and the stellar wind (see the review by Dubus 2013), and both Waisberg & Romani (2015) and Strader et al. (2015) favour a neutron star as the compact companion. We adopt the position and size of the SNR from Green (2019). Ruiz & May (1986) estimate an age of 10^4 yr.

A10 G296.5+10.0

G296.5+10.0 is associated with the X-ray PSR J1210−5226 (Zavlin et al. 2000). Halpern & Gotthelf (2015) measure a proper motion of $(-12 \pm 5, 9 \pm 8)$ mas yr^{-1}. Giacani et al. (2000) estimate a distance of $2.1^{+1.8}_{-0.8}$ kpc, so we adopt a 'parallax' of $\varpi = 0.50 \pm 0.25$. We adopt the centre and diameter (76′) from Green (2019). Roger et al. (1988) estimate an age of 7000 yr with uncertainties of a factor of 3. de Luca et al. (2004) find $N(H) = (1.3 \pm 0.1) \times 10^{21}$ cm^2, corresponding to $E(B - V) \simeq 0.22 \pm 0.02$, so for a distance of 4 kpc, we can probe down to $>2\,M_{\odot}$.

This paper has been typeset from a TEX/LATEX file prepared by the author.